Research article

Yunhong Ding*, Zhao Cheng, Xiaolong Zhu, Kresten Yvind, Jianji Dong, Michael Galili, Hao Hu, N. Asger Mortensen, Sanshui Xiao and Leif Katsuo Oxenløwe

Ultra-compact integrated graphene plasmonic photodetector with bandwidth above 110 GHz

https://doi.org/10.1515/nanoph-2019-0167
Received June 7, 2019; revised August 9, 2019; accepted August 13, 2019

Abstract: Graphene-based photodetectors, taking advantage of the high carrier mobility and broadband absorption in graphene, have recently seen rapid development. However, their performance with respect to responsivity and bandwidth is still limited by the weak light-graphene interaction and large resistance-capacitance product. Here, we demonstrate a waveguide-coupled integrated graphene plasmonic photodetector on a silicon-on-insulator platform. Benefiting from plasmon-enhanced graphene-light interaction and subwavelength confinement of the optical energy, a small-footprint graphene-plasmonic photodetector is achieved working at the telecommunication window, with a large a bandwidth beyond 110 GHz and a high intrinsic responsivity of 360 mA/W. Attributed to the unique electronic band structure of graphene and its ultra-broadband absorption, operational wavelength range extending beyond mid-infrared, and possibly further, can be anticipated. Our results show that the combination of graphene with plasmonic devices has great potential to realize ultra-compact, high-speed optoelectronic devices for graphene-based optical interconnects.

Keywords: photodetector; graphene; plasmonic waveguide.

***Corresponding author: Yunhong Ding,** Department of Photonics Engineering, Technical University of Denmark, 2800 Kongens Lyngby, Denmark; and Center for Silicon Photonics for Optical Communication (SPOC), Technical University of Denmark, 2800 Kongens Lyngby, Denmark, e-mail: yudin@fotonik.dtu.dk. https://orcid.org/0000-0002-6823-4722
Zhao Cheng: Department of Photonics Engineering, Technical University of Denmark, 2800 Kongens Lyngby, Denmark; and Wuhan National Laboratory for Optoelectronics, Huazhong University of Science and Technology, Wuhan 430074, China
Xiaolong Zhu: Department of Micro- and Nanotechnology, Technical University of Denmark, DK-2800 Kongens Lyngby, Denmark
Kresten Yvind, Michael Galili, Hao Hu and Leif Katsuo Oxenløwe: Department of Photonics Engineering, Technical University of Denmark, 2800 Kongens Lyngby, Denmark; and Center for Silicon Photonics for Optical Communication (SPOC), Technical University of Denmark, 2800 Kongens Lyngby, Denmark
Jianji Dong: Wuhan National Laboratory for Optoelectronics, Huazhong University of Science and Technology, Wuhan 430074, China
N. Asger Mortensen: Center for Nano Optics and Danish Institute for Advanced Study, University of Southern Denmark, Campusvej 55, DK-5230 Odense M, Denmark; and Center for Nanostructured Graphene (CNG), Technical University of Denmark, DK-2800 Kongens Lyngby, Denmark
Sanshui Xiao: Department of Photonics Engineering, Technical University of Denmark, 2800 Kongens Lyngby, Denmark; and Center for Nanostructured Graphene (CNG), Technical University of Denmark, DK-2800 Kongens Lyngby, Denmark

1 Introduction

The fast development of silicon photonics makes it feasible to construct optical interconnects that can replace electrical interconnects for chip-level data communications with low energy consumption and large bandwidth [1, 2]. However, for photodetection in the silicon-based optical interconnect, it still needs to be integrated with another absorbing material, e.g. germanium or a III-V compound semiconductor [3, 4], leaving a big challenge for direct monolithic integration with the complementary metal-oxide-semiconductor (CMOS) technology and in achieving high bandwidth limited by the absorbing materials' poor electrical properties. Graphene, a unique CMOS-compatible, two-dimensional (2D) material, provides great potential in the realization of high-performance optoelectronic devices [5–10]. In particular, significant efforts have been devoted to graphene photodetectors (PDs) [11–21]. The distinct properties of graphene in terms of ultrahigh carrier mobility [22, 23], zero bandgap property, which enables wavelength-independent light absorption over a very wide spectral range [24–26], and tunable optoelectronic properties [27, 28] enable the realization of graphene PDs with a large spectral bandwidth and high speed.

Graphene PDs rely on devices with broken inversion symmetry [11, 12, 29]. For graphene-based integrated

PDs, the inversion symmetry can be conveniently relaxed through an asymmetric positioning of the waveguide with respect to the graphene coverage, and several devices [12, 30] have been reported. However, because of the modest light-matter interaction between the single-layer graphene (SLG) and the waveguide mode, the size of the devices has to be tens to hundreds of micrometers to achieve a reasonable responsivity, thus limiting high-speed operation. A small device, however, gives weak absorption of light and, thus, eventually low responsivity. This counteracting effect represents a big challenge for graphene-based PDs supporting both high responsivity and large bandwidth. The typical bandwidth of the graphene PD is ~76 GHz, however with a modest responsivity of 1 mA/W [31]. Another promising scheme is to break the symmetry of the potential profile of the device by different metallic-induced doping [32] near the metal-graphene contact regions. In this scheme, an internal (built-in) electric field [33] is formed to separate the photogenerated carriers [11, 34]. A milestone for high-speed photodetectors based on SLG has been demonstrated by the free-space top-illumination technique [11]. However, the internal built-in electric field exists only in narrow regions of ~200 nm adjacent to the electrode/graphene interfaces [11, 34]. The large distance of 1 μm between the two electrodes [11] limits the collection efficiency of photogenerated carriers and thus the responsivity. Moreover, the required graphene of very high quality typically relies on the exfoliation method [33], which restricts the potential for large-scale integration.

In order to improve the performance, plasmonic bowtie nanostructure has recently been employed to enhance the light-graphene interaction in a extremely localized area, resulting in larger bandwidth [19]. Here, we report an ultra-compact, on-chip, high-speed graphene photodetector based on a plasmonic slot waveguide [7, 35, 36]. The subwavelength confinement of the plasmonic mode gives rise to enhanced light-graphene interactions, and the narrow plasmonic slot of 120 nm enables short drift paths for the photogenerated carriers. A small integrated graphene photodetector with a graphene coverage length of 2.7 μm is demonstrated without any drop in response up to a frequency of 110 GHz and an intrinsic responsivity of 25 mA/W. Increasing the device size to 19 μm results in an increased intrinsic responsivity of 360 mA/W, equivalent to a high external quantum efficiency of 29%. These performances can further be improved significantly. With the extremely broad absorption band of graphene, our device shows great potential. Moreover, the use of graphene grown here by chemical vapor deposition (CVD) allows scalable fabrication, and we believe that our work greatly pushes the 2D material toward practical applications, e.g. in optical interconnects, high-speed optical communication, and so on.

2 Results

2.1 Principle

The schematic of the proposed graphene-plasmon hybrid photodetector is shown in Figure 1A, where the light from a fiber is first coupled to a silicon waveguide through a grating coupler [37] and further to the plasmonic slot

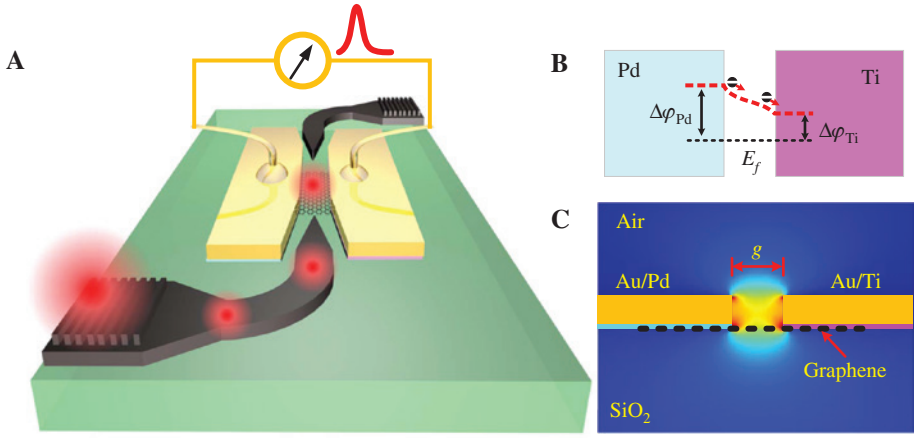

Figure 1: Principle of the graphene-plasmonic integrated photodetector.
(A) Schematic of the proposed graphene-plasmonic hybrid photodetector. (B) The potential profile of the device showing the drift of the photogenerated carrier. $\Delta\phi_{Pd}$ and $\Delta\phi_{Ti}$ are the difference between the Dirac point energy and the Fermi level in palladium- and titanium-doped graphene, respectively. (C) Cross-section of the device with its corresponding plasmonic slot mode at $\lambda = 1.55$ μm.

waveguide by a short tapered structure [7, 36]. The plasmonic slot waveguide (see the cross-section of the device in Figure 1C) consists of two asymmetric metallic contacts of Au(90 nm)/Pd(5 nm) and Au(90 nm)/Ti(5 nm), resulting in different doping levels in the graphene [11]. Photocurrent can be generated from contributions by photothermoelectric (PTE), photobolometric (PB), and photovoltaic (PV) effects. The proposed device, which follows the principle in [11], utilizes the PV current as the dominant contribution. The PTE effect is due to temperature gradient in the device and to the doping asymmetry. The generated photocurrent is proportional to $(S_2–S_1)\mathrm{d}T/\mathrm{d}x$, where S_1 and S_2 are the Seebeck coefficients for the two metal-graphene contacts. In the proposed device, though the different metallic doping introduces a difference in the Seebeck coefficients, the whole graphene layer is illuminated by light within the narrow plasmonic gap, resulting in a near-zero net temperature gradient and thus negligible PTE current. The PB response of the graphene photodetector can be observed only in biased devices. However, as we do not have a gating voltage, and the graphene is under low doping, this results in a negligible PB current [38]. Thus the PV current is the only known dominant contribution. The potential difference indicated in Figure 1B gives rise to efficient separation of the photgenerated carriers and formation of the photocurrent. The performance with respect to responsivity and speed of the proposed photodetector really takes advantage of the plasmonic slot waveguide with the narrow gap g of 120 nm. First, the plasmonic slot waveguide provides subwavelength light confinement in the nanometer scale, as shown in Figure 1C, resulting in extremely strong graphene-light interaction and thus high responsivity. With the optimum geometry with a small gap and thin Au layer of the plasmonic slot waveguide, the single-layer graphene leads to extremely high light absorption of ~1 dB/μm (see the Supplementary Material), which is at least one order of magnitude higher than that of graphene-silicon waveguide photodetectors [12, 31]. Second, the internal electric field mentioned above covers the whole plasmonic slot region of 120 nm. Thus, the photogenerated carriers can be effectively separated, leading to high responsivity. Furthermore, the narrow plasmonic slot gives short drift paths for carriers, resulting in ultrafast carrier transition through the photodetection region and thus high speed.

2.2 Experimental results

Figure 2A shows the fabricated graphene-plasmonic photodetector, where the dashed lines represent the graphene coverage boundary. The Raman spectrum shown in Figure 2B illustrates moderate degradation after the wet-transfer process, which is given in Section 4.2. Graphene-plasmonic hybrid photodetectors with different graphene coverage lengths were fabricated, and the cut-back method shows absorption coefficient of 0.8 dB/μm in the detection region, as presented in Figure 2C.

Being a key parameter, the intrinsic responsivity R_{ph} of the graphene-plasmonic waveguide photodetector with respect to the power in the plasmonic waveguide was characterized with a light power of −4 dBm (400 μW) in the plasmonic waveguide. The photocurrent was measured by switching on and off the light, and the current difference was recorded. Measurements were performed at different bias voltages V_B (Au/Ti electrode relative to Au/Pd electrode) for devices with different graphene-coverage lengths L (=2.7, 3.5, 9.0, 19 μm), as shown in Figure 3A. The potential profile at different bias voltages and the corresponding output electrical signals, due to the injection of an optical pulse into the chip, are also presented in Figure 3B and C, respectively. At zero bias voltage, an intrinsic responsivity of ~1.3 mA/W is observed for the device with the graphene coverage length of 19 μm (see the inset of Figure 3A). It is due to the asymmetric potential profile between the two electrodes, which is also addressed in [11]. The zero responsivity measured at the negative bias around −0.1 V indicates a flat potential profile, as presented in Figure 3B, and no change in the optical signal is observed (see the second subplot in Figure 3C). Further increasing the negative bias voltage results in an increased responsivity, and a clear electrical pulse is obtained at −0.8 V (Figure 3C). Increasing the positive bias voltage also causes an increase in the responsivity and a clear output electrical pulse with opposite polarity compared to the negative biasing case. A bias voltage beyond 1.5 V leads to a significant increase in responsivity and much larger amplitude for the electrical pulse. Moreover, as the graphene coverage length L increases, an improvement in the responsivity is also observed, as shown in the inset of Figure 3A, since a larger fraction of optical power is absorbed, thereby leading to a higher photocurrent. As presented in Figure 3A, the smallest device with 2.7 μm graphene coverage gives a responsivity of ~26 mA/W at the bias voltage of 2 V. The quantum yield is represented by the external quantum efficiency (EQE), which defined by $\mathrm{EQE} = R_{\mathrm{ph}} \times \hbar\omega/e$, where $\hbar\omega$ is the photon energy ($\hbar$ being the Planck constant and ω the frequency of light), and e is the electronic charge. Thus, the corresponding EQE of 2% is obtained. For the device with 19 μm graphene coverage, the highest responsivity of 360 mA/W is

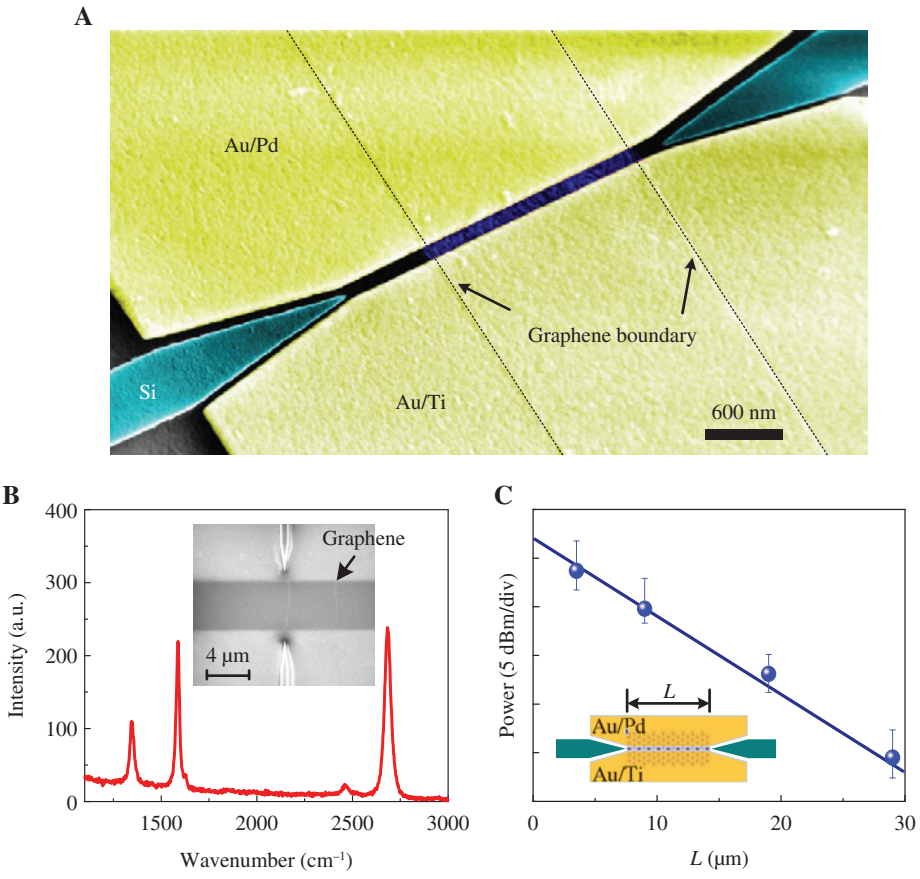

Figure 2: Characterization of the fabricated device.
(A) Example of fabricated graphene plasmonic photodetector with the graphene coverage length of 2.7 μm. (B) Measured Raman spectrum for the graphene after the wet-transfer process. The inset shows the scanning electron microscope (SEM) image of the device with 2.7 μm after the graphene patterning process. (C) Analysis of coupling and propagation loss by the cut-back method. The error bar is obtained by measuring six copy devices with the same graphene coverage length.

obtained with the bias voltage of 2.2 V, corresponding to a high EQE of 29%.

We further measured the bandwidth of these graphene-plasmonic photodetectors, as presented in Figure 4A–D. The experimental setup can be found in the Supplementary Material. All measurements were carried out with the bias voltage of 1.6 V to get a good signal-to-noise ratio. At low frequency (below 40 GHz), we used a vector network analyzer (VNA, 40 GHz bandwidth) to measure the current (optical) frequency response R_{op}. No response drop is found within the 40 GHz bandwidth (the blue lines in Figue 4A–D), indicating a large detection bandwidth. Then, the devices were further characterized by the alternative method of fast Fourier transform (FFT) of the impulse response of the detectors. Within the 40 GHz bandwidth, the frequency response obtained by the impulse response method (see the red solid red lines) agrees quite well with that of the VNA method mentioned above. With the aid of the impulse response method, we obtain the measurement system optical bandwidth of at least 85 GHz for the smallest device with the graphene coverage length of 2.7 μm. Increasing the device size results in a broader impulse response (see the Supplementary Material) and thus a smaller bandwidth. The device with a graphene coverage length of 19 μm exhibits the measurement system's optical bandwidth of at least 75 GHz. All the impulse response measurements for the devices can be found inthe Supplementary Material. Note that such systematic bandwidth is significantly influenced by the bandwidth of the oscilloscope, the RF cable, and the bias Tee. Thus, we have employed the third method (FB + ESA) utilizing frequency beating (FB) between two coherent light fields to measure the RF power in a wideband electrical spectral analyzer (ESA, 110 GHz bandwidth). As presented in Figure 4A–D, for the frequency near 40 GHz, the response obtained by the FB + ESA method (triangular marks) overlaps quite well with that obtained by the VNA method (blue curves). Within 110 GHz, no drop in detection response is

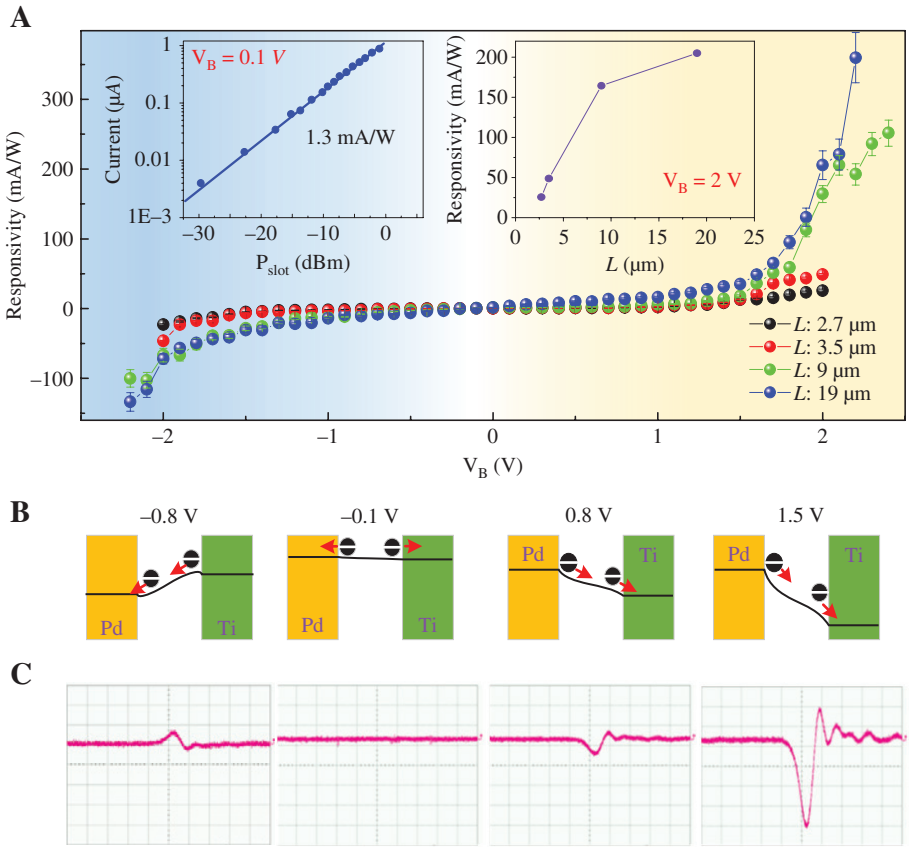

Figure 3: Characterization of responsivity of the devices.
(A) Measured responsivity at different bias voltages for four devices with different *L*. The insets show the measured photocurrent as a function of the light power with zero bias, as well as the responsivity versus the graphene coverage length *L* with bias voltage of 2 V. (B) Schematics of the potential profiles at different biases. (C) The corresponding measured output electrical signals for the photodetector with graphene coverage length *L* of 19 μm. The time scale is 20 ps/div.

observed for the device with a graphene coverage length of 2.7 μm, indicating a bandwidth >110 GHz. A longer device leads to a slight drop in the detection response at high frequencies (~100 GHz). The small frequency dip at ~46 GHz is attributed to the impedance mismatch between the electrode pads and the RF probe. The device with a graphene coverage length of 19 μm (Figure 4D) exhibits a 1.5-dB optical bandwidth of 110 GHz. With the increase of the graphene coverage length, the responsivity is significantly improved, as demonstrated in Figure 3A, while the current frequency response R_{op} (shown by the red triangular marks) at the high frequency slightly drops, indicating a tradeoff between responsivity and bandwidth.

The detector with graphene coverage length of 19 μm was further used to receive 10, 20, and 40 Gbit/s return-to-zero (RZ) optical signals with a pseudo-random binary sequence (PRBS) length of 2^{31}–1, which is amplified by an erbium-doped fiber amplifier (EDFA) and injected into the chip. The output electrical signal from the graphene photodetector was electrically amplified (40 GHz bandwidth electrical amplifier) and fed to the high-speed oscilloscope (70 GHz bandwidth) to record the eye diagram. Clear and open eye diagrams were obtained for all signal (10, 20, and 40 Gbit/s), as shown in Figure 4E–G, indicating no pattern effect of the detector and proving the feasibility of using such graphene photodetectors in realistic optical communication applications.

3 Conclusion and discussion

In summary, we have demonstrated an on-chip, ultra-high-bandwidth photodetector based on a single-layer CVD graphene and plasmonic slot waveguide hybrid structure. The narrow plasmonic slot waveguide not only enhances light-graphene interactions but also enables the effective separation of the photogenerated carriers, leading to high responsivity and large bandwidth. An optical bandwidth larger than 110 GHz with large responsivity of 360 mA/W has been achieved. With narrower plasmonic gap as

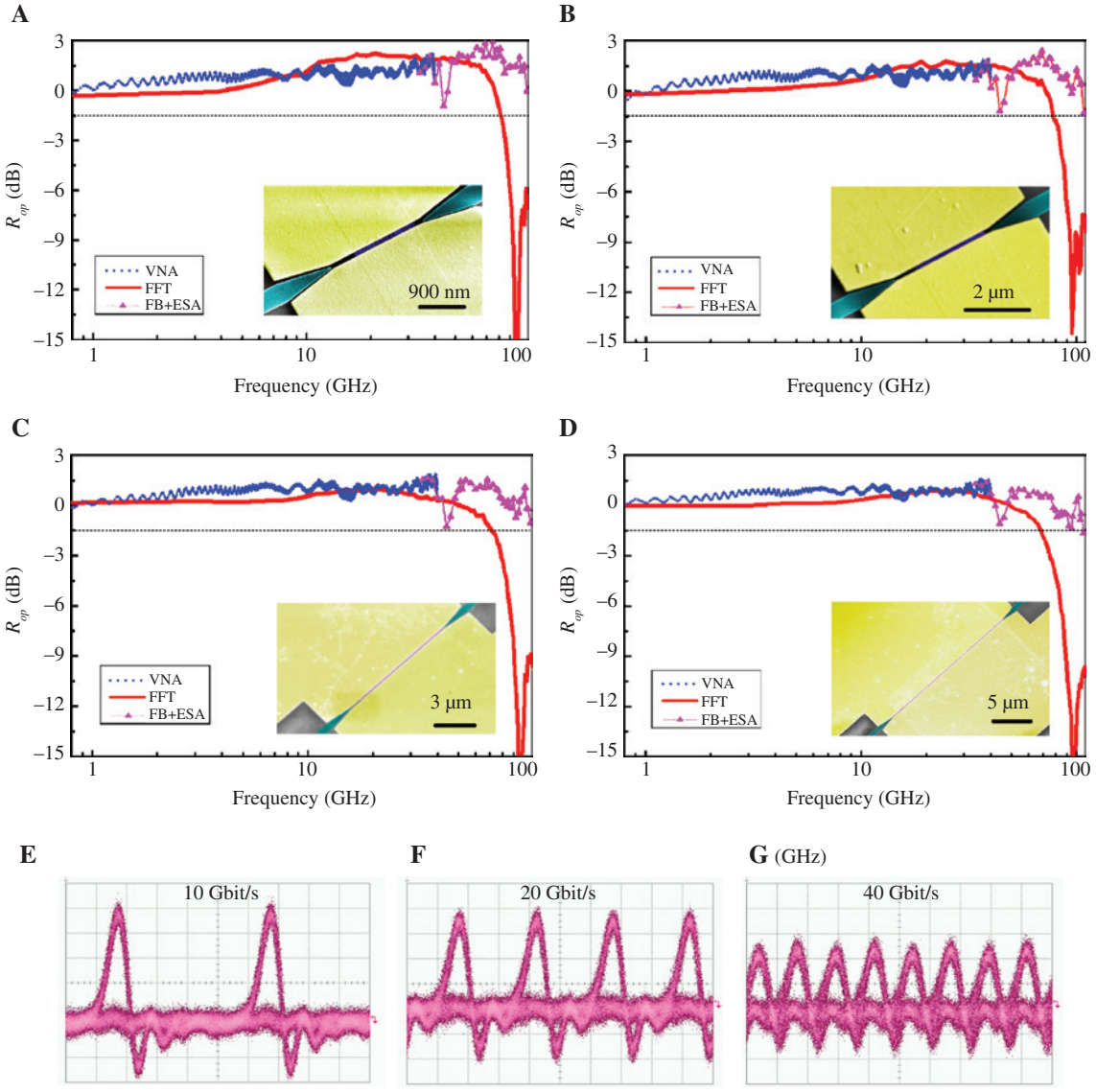

Figure 4: Bandwidth characterization of the devices.
(A–D) Measured optical bandwidth by VNA, impulse response, and frequency beating with ESA for the devices with graphene coverage lengths of 2.7, 3.5, 9, and 19 μm, respectively, at the bias voltage of 1.6 V. The insets show the SEM images of associated fabricated devices. (E–G) Measured eye diagram of the RZ optical signal at 10, 20, and 40 Gbit/s, respectively, for the device with 19 μm graphene coverage length and biased at 1.6 V.

well as thinner Au layer, higher absorption by graphene is expected, thus promising even higher responsivity, as analyzed in the Supplementary Material. Furthermore, tuning the Fermi level by the top gate [16] would further improve the absorption of graphene and thus the responsivity. Moreover, the use of CVD-grown graphene enables large-scale integration.

It should be noted that the narrow plasmonic slot of 120 nm results in an ultrafast transit of carriers to the electrodes. The transit-time-limited bandwidth of the photodetector is given by $f_t = 3.5/2\pi t_{tr}$ [34], where t_{tr} is the transit time through the photodetection region. The carrier velocity can be estimated by a typical fitting function presented in [39]. The saturation carrier velocity ranges from 1×10^7 cm/s [39] to 5.5×10^7 cm/s [40]. Here we consider a relatively conservative carrier velocity of 1.4×10^7 cm/s. At zero bias voltage, the difference in Fermi level between the palladium- and titanium-doped graphenes is 0.05 V [11], resulting in the built-in electric field of ~0.4 V/μm. With a typical carrier mobility of 4×10^3 cm/Vs for CVD graphene on SiO_2 and a fitting parameter $\gamma = 3$, a corresponding carrier velocity of 1.1×10^7 cm/s is obtained, which

means that it takes only 1.1 ps for the carriers to transit through the 120-nm plasmonic slot gap. Thus, a single transit-time-limited bandwidth of 520 GHz is expected. The capacitance of the photodetector can be estimated by taking a similar photodetector of plasmonic slot with amorphous germanium [36] for reference, where the capacitance was measured to be 5 fF with a 20-μm-long plasmonic slot waveguide of 100-nm-thick Au and 160 nm gap. Thus a capacitance of 0.83 and 6.7 fF is estimated for our device with graphene coverage lengths of 2.5 and 19 μm, respectively. The resistance is composed of the serier resistances by Ti-graphene and Pd-graphene contacts and a loading resistance of 50 Ω. A conservative contact resistivity of 1000 Ωμm [41] is used, corresponding to a total contact resistance of 800 and 100 Ω for the devices with graphene coverage lengths of 2.5 and 19 μm, respectively, resulting in bandwidths of 150 and 220 GHz, which are both smaller than the transit-time-limted bandwidth. Actually, one could find a slight frequency response drop around 100 GHz when the graphene coverage length changes from 2.5 to 19 μm, as shown in Figure 4, which is consistant with the analysis above. Further optimizing the contact resisance and Au thickness would help increase the bandwidth.

In this work, the devices were characterized around 1540 nm. In terms of optical absorption bandwidth, research has shown that graphene exhibits ultrawide band absorption from the terahertz to the visible range [25]. Ultra-broad-band photodetection has also been demonstrated from 800 nm up to 20 μm [26]. The only restriction of the optical wavelength bandwidth is the inverse taper coupling bandwidth from the silicon waveguide to the plasmonic slot waveguide. Nevertheless, previous works have shown that such coupling bandwidth is at least 100 nm [42, 43]. This suggests that our device could work over a broad wavelength range. The devices demonstrated here are fully CMOS-compatible and can easily be integrated with the silicon platform, and the use of CVD-grown graphene shows a promising way to achieving multifunctional integrated graphene devices for optical interconnects.

4 Method

4.1 Fabrication process

The device was fabricated on a commercial silicon-on-insulator sample with a top silicon layer of 250 nm and a buried oxide layer of 3 μm. The top silicon layer was first thinned down to 100 nm by dry etching (STS advanced-silicon-etching machine, ASE) in order to obtain good coupling efficiency with the plasmonic slot waveguide. The grating couplers and silicon waveguides were patterned by electron beam lithography (EBL, E-Beam Writer JBX-9500FSZ), and fully etched by the ASE dry-etching process. After that, the graphene layer was wet-transferred and patterned by standard ultraviolet (UV) lithography (Aligner: MA6-2) and oxygen (O_2) plasma etching. Then, the Au/Pd (90 nm/3 nm)-graphene contact was patterned by a second EBL process, followed by metal deposition and lift-off. Finally, the Au/Ti (90 nm/3 nm)-graphene contact was patterned by a third EBL step, followed by metal deposition and lift-off.

4.2 Graphene wet-transfer process

SLG grown by CVD on a Cu foil (GRAPHENE SUPERMARKET) was transferred onto the devices by a wet-chemistry method. The SLG sheet was transferred by the following steps. First, a layer of photoresist (AZ5200 series) was spin-coated (3500 rpm for 1 min) onto the SLG, and the photoresist/SLG stack was then released by etching the underlying Cu foil in a $Fe(NO_3)_3$ solution (17 wt%) at room temperature. The stack floating in the solution was then washed by deionized (DI) water a couple of times and transferred to the target device, followed by drying at room temperature for at least 24 h. Afterward, the photoresist on the SLG was dissolved in acetone at room temperature. Finally, the graphene device was cleaned by ethanol and DI water and then dried before further processing.

5 Supplementary Materials

Experimental setup.
Impulse response of the fabricated photodetector.
Simulation of graphene absorption.

Acknowledgments: The authors would like to thank Vitaliy Zhurbenko for the help in calibrating the RF cables and Bias Tee. They thank Prof. Fengnian Xia and Dr. Peter David Girouard for constructive discussion. This work was supported by the Center for Silicon Photonics for Optical Communication (SPOC, DNRF123, Funder Id: http://dx.doi.org/10.13039/501100001732) and the Center for Nanostructured Graphene (CNG, DNRF103, Funder Id: http://dx.doi.org/10.13039/501100001732), both sponsored by the Danish National Research Foundation; the QUANPIC project

sponsored by VILLUM FONDEN (ref 00025298, Funder Id: http://dx.doi.org/10.13039/100008398); the Independent Research Fund Denmark (Project No. 9041-00333B, Funder Id: http://dx.doi.org/10.13039/501100011958), and the mid-chip project sponsored by VILLUM FONDEN (No. 13367, Funder Id: http://dx.doi.org/10.13039/100008398). N.A.M. is a VILLUM Investigator supported by VILLUM FONDEN (No. 16498, Funder Id: http://dx.doi.org/10.13039/100008398) and X.Z. is supported by VILLUM Experiment (No. 17400, Funder Id: http://dx.doi.org/10.13039/100008398).

Conflict of interest: The authors declare no conflict of interests. A recent post in arxiv by Z. Ma et al. has shown that significant enhancement of responsivity can be achieved when further decreasing the plasmonic gap down to 15 nm. Their data further supports the use of the proposed plasmonic slot waveguide for high performance graphene photodetectors.

References

[1] Saraswat KC, Mohammadi F. Effect of scaling of interconnects on the time dealy of VLSI circuits. IEEE Trans Electron Devices 1982;4:645–50.
[2] Miller DA. Device requirements for optical interconnects to silicon chips. Proc IEEE 2009;97:1166–85.
[3] Michel J, Liu J, Kimerling LC. High-performance Ge-on-Si photodetectors. Nat Photon 2010;4:526–34.
[4] Ito H, Kodama S, Muramoto Y, Furuta T, Nagatsuma T, Ishibashi T. High-speed and high-output InP-InGaAs unitraveling-carrier photodiodes. IEEE J Sel Top Quantum Electron 2004;10:709–27.
[5] Liu M, Yin X, Ulin-Avila E, et al. A graphene-based broadband optical modulator. Nature 2011;474:64–7.
[6] Sorianello V, Midrio M, Contestabile G, et al. Graphene-silicon phase modulators with gigahertz bandwidth. Nat Photon 2018;12:40–4.
[7] Ding Y, Guan X, Zhu X, et al. Effective electro-optic modulation in lowloss graphene-plasmonic slot waveguides. Nanoscale 2017;9:15576–81.
[8] Gu T, Petrone N, McMillan JF, et al. Regenerative oscillation and four-wave mixing in graphene optoelectronics. Nat Photon 2012;6:554–9.
[9] Yan S, Zhu X, Frandsen LH, et al. Slow-light-enhanced energy efficiency for the graphene microheater on silicon photonic crystal waveguides. Nat Commun 2017;8:14411.
[10] Sun Z, Hasan T, Torrisi F, et al. Graphene mode-locked ultrafast laser. Nano Lett 2010;4:803–10.
[11] Mueller T, Xia F, Avouris P. Graphene photodetectors for high-speed optical communications. Nat Photon 2010;4:297–301.
[12] Gan X, Shiue R-J, Gao Y, et al. Chip-integrated ultrafast graphene photodetector with high responsivity. Nat Photon 2013;7:883–7.
[13] Pospischil A, Humer M, Furchi MM, et al. CMOS-compatible graphene photodetector covering all optical communication bands. Nat Photon 2013;7:892–6.
[14] Wang X, Cheng Z, Xu K, Tsang HK, Xu J-B. High-responsivity graphene/silicon-heterostructure waveguide photodetectors. Nat Photon 2013;7:888–91.
[15] Schall D, Neumaier D, Mohsin M, et al. 50 GBit/s photodetectors based on wafer-scale graphene for integrated silicon photonic communication systems. ACS Photon 2014;1:781–4.
[16] Liu C-H, Chang Y-C, Norris TB, Zhong Z. Graphene photodetectors with ultra-broadband and high responsivity at room temperature. Nat Nanotechnol 2014;9:273–8.
[17] Schuler S, Schall D, Neumaier D, et al. Controlled generation of a p-n junction in a waveguide integrated graphene photodetector. Nano Lett 2016;16:7107–12.
[18] Goykhman I, Sassi U, Desiatov B, et al. On-chip integrated, silicon-graphene plasmonic Schottky photodetector with high responsivity and avalanche photogain. Nano Lett 2016;16:3005–13.
[19] Ma P, Salamin Y, Baeuerle B, et al. Plasmonically enhanced graphene photodetector featuring 100 GBd, high-responsivity and compact size. ACS Photon 2018;6:154–61.
[20] Schall D, Pallecchi E, Ducournau G, Avramovic V, Otto M, Neumaie D. Record high bandwidth integrated graphene photodetectors for communication beyond 180 Gb/s. In: Optical fiber communication conference (OFC'2018), OSA Technical Digest (online) (Optical Society of America, 2018), San Diego, CA, USA, paper M2I.4, 2018.
[21] Flöry N, Ma P, Salamin Y, et al. Waveguide-integrated van der Waals heterostructure photodetector at telecom band with high speed and high responsivity. 2018;arXiv:1904.10287.
[22] Bolotina KI, Sikes KJ, Jiang Z, et al. Ultrahigh electron mobility in suspended graphene. Solid State Commun 2008;146:351–5.
[23] Dorgan VE, Bae M-H, Pop E. Mobility and saturation velocity in graphene on SiO_2. Appl Phys Lett 2010;97:082112.
[24] Nair RR, Blake P, Grigorenko AN, et al. Fine structure constant defines visual transparency of graphene. Science 2008;320:1308.
[25] Dawlaty JM, Shivaraman S, Strait J, et al. Measurement of the optical absorption spectra of epitaxial graphene from terahertz to visible. Appl Phys Lett 2008;93:131905.
[26] Cakmakyapan S, Lu PK, Navabi A, et al. Goldpatched graphene nano-stripes for high-responsivity and ultrafast photodetection from the visible to infrared regime. Light Sci Appl 2018;7:20.
[27] Li ZQ, Henriksen EA, Jiang Z, et al. Dirac charge dynamics in graphene by infrared spectroscopy. Nat Phys 2008;4:532–5.
[28] Wang F, Zhang Y, Tian C, et al. Gate-variable optical transitions in graphene. Science 2008;320:206–9.
[29] Koppens FHL, Mueller T, Avouris P, et al. Photodetectors based on graphene, other two-dimensional materials and hybrid systems. Nat Nanotechnol 2014;11:780–93.
[30] Shiue R-J, Gao Y, Wang Y, et al. High-responsivity graphene-boron nitride photodetector and autocorrelator in a silicon photonic integrated circuit. Nano Lett 2015;15:7288–93.
[31] Schall D, Porschatis C, Otto M, Neumaier D. Graphene photodetectors with a bandwidth >76 GHz fabricated in a 600 wafer process line. J Phys D: Appl Phys 2017;50:124004.

[32] Giovannetti G, Khomyakov PA, Brocks G, et al. Doping graphene with metal contacts. Phys Rev Lett 2008;101:026803.
[33] Novoselov KS, Geim AK, Morozov SV, et al. Electric field effect in atomically thin carbon films. Science 2004;306:666–9.
[34] Xia F, Mueller T, Ming Lin Y, Valdes-Garcia A, Avouris P. Ultrafast graphene photodetector. Nat Nanotechnol 2009;4:839–43.
[35] Ayata M, Fedoryshyn Y, Heni W, et al. High-speed plasmonic modulator in a single metal layer. Science 2017;358:630–2.
[36] Salamin Y, Ma P, Baeuerle B, et al. 100 GHz plasmonic photodetector. ACS Photon 2018;5:3291–7.
[37] Ding Y, Ou H, Peucheret C. Ultra-high-efficiency apodized grating coupler using fully etched photonic crystals. Opt Lett 2013;38:2732–4.
[38] Freitag M, Low T, Xia F, Avouris P. Photoconductivity of biased graphene. Nat Photon 2013;7:53–9.
[39] Bonmann M, Vorobiev A, Andersson MA, Stake J. Charge carrier velocity in graphene field-effect transistors. Appl Phys Lett 2017;111:233505.
[40] Meric I, Han MY, Young AF, Ozyilmaz B, Kim P, Shepard KL. Current saturation in zero-bandgap, top-gated graphene field-effect transistors. Nat Nanotechnol 2008;3:654–9.
[41] Kovacevic G, Phare C, Set SY, Lipson M, Yamashita S. Ultra-high-speed graphene optical modulator design based on tight field confinement in a slot waveguide. Appl Phys Express 2018;11:065102.
[42] Ono M, Taniyama H, Xu H, et al. Deep-subwavelength plasmonic mode converter with large size reduction for Si-wire waveguide. Optica 2016;3:999–1005.
[43] Tian J, Yu S, Yan W, Qiu M. Broadband high-efficiency surface-plasmon-polariton coupler with silicon-metal interface. Appl Phys Lett 2009;95:013504.

Supplementary Material: The online version of this article offers supplementary material (https://doi.org/10.1515/nanoph-2019-0167).